Elastic Properties of Nonstoichiometric Reacted PDMS Networks

A. L. Larsen,*,† K. Hansen,† P. Sommer-Larsen,‡ O. Hassager,† A. Bach,† S. Ndoni,‡ and M. Jørgensen‡

The Danish Polymer Centre, Department of Chemical Engineering, Technical University of Denmark, DK-2800 Kgs. Lyngby, Denmark, and Risø National Laboratory, DK-4000 Roskilde, Denmark

Received March 20, 2003; Revised Manuscript Received October 8, 2003

ABSTRACT: The influence of stoichiometry on the elastic modulus of eight-functional end-linked poly(dimethylsiloxane) (PDMS) networks was investigated by extensional rheometry with extensions up to more than 100%, and the stress−strain relation was found to be almost linear—a characteristic property for a network structure with an eight-functional cross-linker. The experimental data were compared to a stochastic model taking into account entanglements and to Monte Carlo simulations. The Mooney−Rivlin model was furthermore used to fit the data, and the dependency of C_1 and C_2 parameters on the stoichiometric ratio was investigated in order to clarify especially the influence of trapped entanglements acting either as chemical cross-links or as sliding links. It was found that including a locking factor dividing trapped entanglements into locked entanglements and slip-links could explain our data obtained for the Mooney−Rivlin constants. It was furthermore found that trapped entanglements dominate when there is an excess of cross-linker, ensuring that all long difunctional DMS chains are bound to the infinite network in both ends.

Introduction

The structures and properties of polymer networks are highly sensitive to the reaction by which they are formed.[1] If absolute values of moduli are to be interpreted meaningfully, a thorough knowledge of imperfections in the network structure introduced by the cross-linking is essential. Types of imperfection occurring naturally in end-linking curing reactions are inelastic loops and dangling substructure formations. Furthermore, trapped entanglements can be regarded as network imperfections enhancing the network modulus. The formation of a perfect network from an end-linking polymerization requires that the pregel intramolecular reaction is negligible and that postgel intramolecular reaction always leads to elastically active chains. These requirements cannot be met in real cross-linking reactions.[1]

There are several ways to investigate the network structures, for example, small-angle neutron scattering,[2] dynamic light scattering,[3] swelling experiments,[2−4] solution and solid-state silicon 29 NMR spectroscopy,[5] and computer simulations.[6,7] Another feasible way of studying the network structure is extensional rheometry which gives information about the cross-link density. The method nevertheless requires a model in order to interpret the results. Two well-proven models are the Mooney−Rivlin (MR)[9] and the Edwards−Vilgis slip-link theory (SL).[10] The MR theory was proposed as a purely phenomenological equation, however, capable of describing extension of rubberlike materials to relatively large extensions. A direct physical interpretation of the $2C_1$ parameters can nevertheless be given. The situation when $C_2 = 0$ equals the well-known phantom model, so the C_1 parameter can be interpreted as the "ideal" part of the network taking into account permanent cross-links (both chemical or physical), whereas the C_2 parameter takes into account imperfections and slip-links. The SL theory is based on the idea that there are two kinds of cross-links in the rubber network: the chemical cross-links which behave like the prediction of the phantom model and the trapped entanglements acting as sliding links. The theory predicts both low-strain softening and high-strain hardening due to the restriction in extensibility caused by the trapped entanglements.

Previous investigations of the influence of functionality and chain length of poly(dimethylsiloxane) (PDMS) networks on the elastic modulus performed by Oppermann and Rehage[11] showed that the phantom model was inadequate. They concluded that at high branching densities the experimentally observed moduli could be as much as 3 times greater than those calculated from the theory of phantom networks. As the branching density decreases, this ratio decreases and tends to approach unity.

Experimental Section

Preparation of Networks. A two-component room temperature vulcanizing silicone was used. The two components were a vinyl-terminated dimethylsiloxane (DMS-V31) and an eight-functional (on average) methylhydrosiloxane−dimethylsiloxane copolymer (HMS-301), both from Gelest, Inc. A platinum catalyst (SiP6830.0 from Gelest, Inc.) was used in the addition reaction. The networks were prepared by mixing half of the needed amount of DMS-V31 with all of the HMS-301. The second half of DMS-V31 was mixed with the catalyst, and finally this mixture was poured into the first one and thoroughly mixed together. For example, a stoichiometric mixture was prepared from 21.36 g of DMS-V31 (∼1 mmol), 0.5 g of HMS-301 (∼0.25 mmol), and 0.5 g of a mixture of 0.1 cm^3 SiP6830.0 catalyst in 50 g of DMS-V31. Air bubbles were removed in a vacuum. The reaction mixtures were poured into straws (4.7−5.0 mm in diameter and approximately 15 cm long) and cured in an oven at 70 °C for 40 min. Then the straws were removed, and the samples were further cured at 150 °C for 30 min. The resulting samples were 15 cm long silicone rubber cylinders with a diameter of approximately 5 mm. Samples were prepared with the mass ratios DMS-V31 to HMS-301 of (15, 20, 25, 30, 33, 35, 40, 43.7, 50), corresponding to stoichiometric imbalances of (2.92, 2.20, 1.76, 1.47, 1.33,

† Technical University of Denmark.
‡ Risø National Laboratory.
* Corresponding author.

10.1021/ma034355p CCC: $25.00
Published on Web 11/21/2003

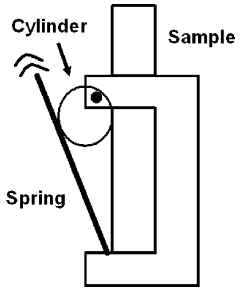

Figure 1. Holder constructed to maintain the pressure on the sample.

1.26, 1.10, 1.01, 0.88); see later for definition. To ensure that the samples prepared at the relatively high temperature (70 °C) did not undergo significant side reactions, two replicates of the 30 mass ratio sample were made, and these samples were cured at ambient temperature for 3 weeks and compared to the samples cured at relatively high temperature.

Extensional Rheometry. We used an in-house-designed filament stretch rheometer. A detailed description of the instrument can be found in ref 12. Two holders (the lower one shown in Figure 1) attached the sample to a load cell in one end and to the moving sledge in the other. Concurrent values of time, load, and sample diameter at the midpoint of the sample were measured at room temperature. The experiments were performed at a constant Hencky strain rate of 0.001 s^{-1}. Typically, 4000 data points were measured for each sample with a sampling frequency of 6.6 per second. We measured the diameter of a slice in the middle of the cylindrical sample. Assuming overall incompressibility, this slice is deforming ideally under elongation. Hence, the local extension ratio in the middle of the sample can be determined from the instantaneous and initial diameters as $\lambda = (D_0/D)^2$. Because of the low strain rate, it is assumed that the sample is in equilibrium during each individual sampling of data points. We may then compute the tensile stress as the normal stress difference: $\sigma_{zz} - \sigma_{rr} = F/(A_0\lambda)$, where A_0 is the initial cross-sectional area of the sample. The stress as a function of relative extension ratio, λ, was fitted to the Mooney−Rivlin model with the NonLinearfit routine in Mathematica 4.1 (Wolfram Research, Inc.). The data were also fitted to a Hooke (linear) model and to a Neo-Hooke model. The goodnesses of the fits were compared using an F-test.[13]

NMR. ^{1}H spectra were obtained on a Bruker Advance DPX-250 spectrometer in $CDCl_3$ at room temperature. ^{1}H chemical shifts were referenced to TMS via the residual nondeuterated solvent signal at $\delta = 7.26$ ppm.

The molar amount of vinyl groups in DMS-V31 per $-CH_3$ group was determined from the ratio between the integrated signals around $\delta = 6.0$ ppm (CH_2═$CH-Si$) and the integrated signal at $\delta = 0$ ppm (CH_3-Si). Number-averaged molecular weights were calculated assuming that both chain ends are vinyl-terminated. The molar amount of silanes in HMS-301 per $-CH_3$ group was determined from the ratio between the integrated signal at $\delta = 4.6$ ppm (H−Si) and the integrated signal at $\delta = 0$ ppm (CH_3-Si). The molar silane amount per chain was calculated assuming a number-averaged molecular weight of 2000 g mol^{-1} and that both ends are methyl-terminated.

Size Exclusion Chromatography (SEC). SEC was used to characterize the molecular weight distribution for DMS-V31. To determine M_n accurately, a small low-molecular-weight fraction was removed by repeated extractions with ethanol and subsequent drying under vacuum. The SEC column system consisted of a PLgel 5 μm Guard 50 mm × 7.5 mm and two PLgel 5 μm Mixed-D 300 mm × 7.5 mm. A Viscotek right angle light scattering model 600 and a Viscotek differential refractometer/viscometer model #200 were used as detectors. The column and the detectors were at room temperature (23.0 ± 0.5 °C), and toluene at 1.0 mL/min was the eluent. A Shimatzu HPLC pump LC-10AD was used. The light scattering and refractometer signals were calibrated to a polystyrene standard (Waters 110 000 Da, part no. 41995) with a polydispersity less than 1.01.

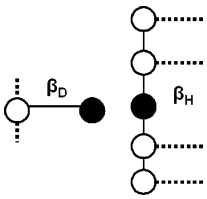

Figure 2. Two different probabilities of a site not being connected to infinity via a particular branch. Subscripts D and H indicate the bifunctional DMS and f-functional HMS chains, respectively.

Network Monte Carlo Simulations. The network structure and elastic modulus were simulated using a Monte Carlo technique. The Networks Monte Carlo module from Accelrys[14−17] was used. DMS-V31 was modeled as end-linked chains. HMS-31 was modeled as a copolymer with the $Si(CH_3)H$ cross-link sites randomly distributed along the chain. A simulation box with volume 10^9 Å^3 contained around 50 000 polymer molecules depending on molecular weight. The polymer molecules was created from a Flory distribution with polydispersity 2 and number-average molecular weight as given in the Results section. The polymers were treated as Gaussian chains and allowed to move around in the simulation box during which the cross-linking reaction was performed. A characteristic ratio of 6.0 was used for both silicone polymers.[18] To check for finite size effects, calculations used to determine the gel point were performed with a 10 times larger box as well (volume of 10^{10} Å^3).

Theory

Several articles in the literature indicate that the strongest networks are not necessarily obtained for stoichiometric mixtures but rather for a mixture with an excess of the f-functional cross-linker compared to the difunctional end-linker for the PDMS network system.[3,19−22] The molar ratio of cross-link sites to precursor polymer ends, $r = f[HMS]_0/(2[DMS]_0)$ (where $[...]_0$ denotes initial concentration), is called the stoichiometric imbalance. For a stoichiometric mixture $r = 1$, in contrast to r_{opt} denoting the value of r for which the modulus is maximal. Patel and Cohen[3] reported values of r_{opt}, which is the value of the stoichiometric imbalance where maximum in the equilibrium modulus is obtained, as large as 1.8−1.9 for slightly entangled systems and reported that r_{opt} increased with increasing molecular weight of the difunctional prepolymer. These observations disagree with the traditional idea that the optimal network is formed when the reactants are reacted stoichiometrically. Patel and Cohen[3] explain the phenomenon with the maximum in weight fraction of elastically active chains at $r = r_{opt}$. Others explain this phenomenon with side reactions.[19,20,22]

Not all material in the network will contribute to the elastic modulus. Soluble material, pendant material, and single-chain loops will not contribute to the elastic modulus. For end-linked networks with functionality 3 or 4, statistical expressions for the fractions of soluble, elastic, and pendant material exist,[23] but for higher functionalities, there are no analytical solutions to our knowledge.

To evaluate the development of the gel during the cross-linking reaction, a stochastical analysis is made. In Figure 2 a sketch of the network can be seen. Let β be the probability that the site is not connected to the infinite network via a particular branch and p be the extent of reaction. β_D is then the probability of an DMS

Table 1. Expressions To Calculate the Mole Fractions of Components Occurring in the Different Network Fractions (i = H, D)

solubles	dangling ends	network	elastic active network
$\beta_i^{f_i}$	$f\beta_i^{f_i-1}(1-\beta_i)$	$1-\beta_i^{f_i}$	$1-f\beta_i^{f_i-1}(1-\beta_i)-\beta_i^{f_i}$

reaction site not being connected to the infinite network via a reaction with an HMS reaction site. β_H is the probability of an HMS reaction site not being connected to the infinite network via a reaction with an DMS reaccction site. f is the functionality of the polymer. Then β^{f-1} is the probability that none of the neighbors' subbranches connect to the infinite network, and $p\beta^{f-1}$ is the probability that the site is connected to neighbor chains but not connected to infinity. Furthermore, the site will not be connected to infinity via that particular branch if the site is not reacted (probability $1 - p$). Introducing the relation $p = p_H = p_D/r$, where p_D and p_H are the extents of reaction with respect to DMS and HMS reaction sites, respectively, and relating the probabilities above given an f-functional HMS chain and a difunctional DMS chain gives

$$\beta_H = p_H\beta_D + (1 - p_H) \tag{1}$$

$$\beta_D = rp_H\beta_H^{f-1} + (1 - rp_H) \tag{2}$$

By eliminating β_D from eqs 1 and 2, an expression for β_H is obtained:

$$0 = \beta_H^{f-1} - \frac{1}{rp_H^2}\beta_H + \frac{1 - rp_H^2}{rp_H^2} \tag{3}$$

Then the different mole fractions of the two components in the different network fractions can be calculated by the expressions in Table 1. In order for a molecule to be a soluble, all its sites need to be nonreacted or not connected to the infinite network; i.e., the mole fraction of soluble material of component i will be given by $x_{sol,i} = \beta_i^{f_i}$. The network fraction $x_{net,i} = 1 - x_{sol,i}$. Dangling material consists of one site connected to the infinite network and the rest not connected, i.e., $x_{de,i} = f\beta_i^{f_i-1}(1 - \beta_i)$. The fraction of elastically active DMS chains will be given by $x_{act,D} = 1 - x_{sol,D} - x_{de,D} = 1 - 2\beta_D(1 - \beta_D) - \beta_D^2$. The static network modulus arising from elastically active DMS chains only can then be calculated:

$$G = \nu_c RT \tag{4}$$

where R is the gas constant, T the absolute temperature, and ν_c is the number density of permanent elastically active DMS chains given by

$$\nu_c = \frac{1 - 2\beta_D(1 - \beta_D) - \beta_D^2}{1 + \frac{n_H M_H}{n_D M_D}}\frac{\rho}{M_D} \tag{5}$$

where M_i and n_i are the molecular weight and mole number of component i, respectively. $(\rho/M_D)/(1 + n_H M_H/n_D M_D)$ is the number density of DMS chains since $M_D \gg M_H$.

To take into account a contribution from so-called trapped entanglements, a simplification is made for our system. Given the entanglement molecular weight for well-entangled, linear DMS of $M_E = 12\,000$ g mol^{-1},[24] it is clear that the lengths of the applied DMS chains ($M_{DMS}/M_E = 1.8$) are relatively short. It is assumed that every chain leads to one entanglement in average. This assumption holds for the type of cross-linking system with very short cross-linkers only. Since we have a melt in equilibrium before the cross-linking reaction, the entanglement density should not change significantly during the cross-linking reaction. If the DMS chain entangle around an HMS chain, it is not regarded as an entanglement since the HMS chains are so short that the "entanglement" will be acting from the chemical cross-link and hence not increase the modulus. To be a trapped entanglement, both entangling DMS chains need to be connected to the infinite network in both ends; i.e., the probability of getting a trapped entanglement is

$$P_{TE} = (1 - \beta_D^2 - 2\beta_D(1 - \beta_D))^2 \tag{6}$$

since $1 - \beta_D^2 - 2\beta_D(1 - \beta_D)$ is the probability of choosing an DMS chain connected to infinity in both ends.

The expression for the storage modulus can then be written as

$$G = \nu_c RT + \left(L_E + \frac{1 - L_E}{(1 + \eta)^2}\right)\frac{P_{TE}}{1 + \frac{n_H M_H}{n_D M_D}}\frac{\rho}{M_D}RT \tag{7}$$

where ν_c is given by eq 5, $\eta = 0.2343$ if the slip-link model is applied, L_E is the fraction of trapped entanglements being "locked", i.e., acting like chemical cross-links, and $1 - L_E$ is the fraction of trapped entanglements acting as slip-links.

According to the slip-link and the Mooney−Rivlin models, the expressions for the reduced modulus $\Phi = t/(\lambda^2 - \lambda^{-1})$[25] as a function of strain are given by

$$\Phi_{SL}(\lambda) = k_B T[N_c + N_s H(\lambda,\eta)] \tag{8}$$

$$\Phi_{MR}(\lambda) = 2C_1 + 2C_2/\lambda \tag{9}$$

where N_c is the cross-link (both chemical and trapped entanglement) density and N_s the slip-link density. $H(\lambda,\eta)$ expresses the deviation from the classical elasticity theory:[10]

$$H(\lambda,\eta) = \frac{\lambda^2}{\lambda^2 + \lambda + 1}\left[\frac{1}{(\lambda + \eta)^2} + \frac{1 + \lambda}{\lambda(1 + \eta\lambda^2)^2}\right] \tag{10}$$

where η is the slippage parameter, which is a relative measure of the freedom of a link to slide. For $\eta = 0$, the N_s entanglements would induce the same strain dependence as the N_c cross-links. A constant value of $\eta = 0.2343$ has been calculated assuming that each slip-link on average can slide as far as the centers of its topologically neighboring links.[26] Edwards and Vilgis[10] argue that for a real network η cannot be fixed, thus admitting variable values of η. Thirion and Weil[25] just consider η as a material parameter.

It can be seen that the slip-link model only reduces to the Mooney−Rivlin equation when $\lambda \to 1$. Relating the three equations above, expressions for the parameters C_1 and C_2 can be obtained:

$$2C_1 = k_B T N_c \tag{11}$$

$$2C_2 = k_B T N_s \frac{1}{(1 + \eta)^2} \tag{12}$$

The modulus is given by

$$G_{MR} = 2C_1 + 2C_2 \tag{13}$$

$$G_{SL} = k_B T\left[N_c + N_s \frac{1}{(1+\eta)^2}\right] \tag{14}$$

From the above equations and eq 7, the MR constants can be written as

$$2C_1 = \nu_c RT + L_E \frac{P_{TE}}{1 + \frac{n_H M_H}{n_D M_D}} \frac{\rho}{M_D} RT \tag{15}$$

$$2C_2 = \frac{1 - L_E}{(1+\eta)^2} \frac{P_{TE}}{1 + \frac{n_H M_H}{n_D M_D}} \frac{\rho}{M_D} RT \tag{16}$$

The slip-link model must be used with great caution to interpret stress/strain data limited to medium extensions as our present data. If the data follow the Mooney−Rivlin model, eqs 11 and 12 show that kTN_s and η cannot be determined independently but only in the combination $kTN_s/(1+\eta)^2$. In fact, a least-squares analysis show that the slip-link model with an optimal choice of $\eta = 0.4$ only differs by 5% in average from the Moonley−Rivlin model in the interval $1 < \lambda < 2$. We measure the area of the sample and calculate the extension from it, but more often the extension is measured from the length of the sample and force divided by unstrained area is analyzed. In that case, systematic errors from the clamped ends deforming differently from the rest of the sample as well as random errors may easily approach 5%. Hence, η cannot be found by fitting the slip-link model to such data. On the other hand, if data over a large range of relative extensions are available, the slip-link model including a finite extensibility parameter can very well fit the experimental data (see ref 27).

Results and Discussion

Table 2 shows the results obtained from NMR and GPC data. Two properties need to be determined accurately: the cross-link density in HMS-301 and the number-average molecular weight of DMS-V31. The measured cross-link density of HMS-301, $x_{CH_3HSiO} = 0.278$ (mole percent of CH_3HSiO groups in the chain), is in good agreement with the manufacturer's data (25−30% CH_3HSiO). The molecular weight given by the manufacturer ($M_n = 2000$ g mol^{-1}) corresponds to an average chain length of 28 Si atoms. Eight of these will be CH_3HSiO groups, but the average distance between the cross-links is then less than one Kuhn step and the HMS-301 can be regarded as an eight-functional cross-linker rather than a polymeric cross-linker. ^{1}H NMR data for DMS-V31 showed a number-average molecular weight of 22 000 g mol^{-1}. By washing several times with ethanol, the original sample was separated into two fractions: a purified high-molecular-weight fraction and a low-molecular-weight fraction contained in the washings. Both fractions were dried for 24 h in a vacuum at 60 °C. All NMR spectra showed only the lines corresponding to vinyl protons and Si−CH_3 protons. ^{1}H NMR analysis of the purified fraction and the washings showed M_n to be 28 000 and 8000 g mol^{-1}, respectively. This corresponds to a 15% content by weight of the low-molecular-weight fraction. More than 10% uncertainty in these numbers may certainly be expected, so for that reason we choose to use values that are compromises between the NMR results and the GPC result. M_n for the purified fraction could be determined with confidence from the combined GPC light scattering and refractometer data. A value of $M_n = 21\,800$ g mol^{-1} was found. Judged from the refractometer data for the original sample, the low-molecular-weight fraction is only 6% of the total mass. This indicates that M_n for the original sample is 20 000 g mol^{-1} and that the low-molecular-weight fraction constitutes 15 mol % (if M_n is taken to be 8000 g mol^{-1}). From the GPC data, a polydispersity index of 1.6 was found for DMS-V31. We choose in the following to work with a value of $M_n = 22\,000$ g mol^{-1} for the original sample used in the network formation, but one must keep in mind that the uncertainty in the structural data is at least 10% and that it influences the discussion about the precise stoichiometry for the networks with maximal elastic modulus.

Table 2. Structural Data from NMR and GPC Measurements[a]

compound	mol % CH_3HSiO	M_n/(g mol^{-1})	mass fraction (%)
HMS-301	27.8 (NMR)		
DMS-V31		22 000 (NMR)	100
original		20 000 (GPC + NMR)[b]	
DMS-V31		28 000 (NMR)	85 (NMR)
high-M_n fraction		21 200 (GPC)	94 (GPC)
DMS-V31		8 000 (NMR)	15 (NMR)
low-M_n fraction			6 (GPC)

[a] The source of data is indicated after each value. [b] Determined from $M_n = 22\,000$ g mol^{-1} for high-M_n fraction and 6% w/w of low $M_n = 8000$ g mol^{-1} fraction.

Experimentally, samples are characterized by the mass ratio of DMS-V31 to HMS-301, m_{DMS}/m_{HMS}, and the stoichiometric imbalance is derived from this ratio: $r = n_{CH_3HSiO}/n_{vinyl} = (x_{CH_3HSiO}/M_{av})/[(2m_{DMS}/m_{HMS})/M_{DMS}]$, where $M_{av} = 70.8$ g mol^{-1} is the average monomer mass for HMS-301 determined from x_{CH_3HSiO} and the manufacturer's M_n(HMS-301) = 2000 g mol^{-1}. M_{av} depends only slightly on M_n for HMS-301. An accurate determination of M_n(DMS-V31) is however crucial in order to determine r precisely. Often-used GPC procedures, where silicone molecular weights are determined on the basis of polystyrene calibration curves, were inadequate for the present study as were also the use of the manufacturer's molecular weight.

The equilibrium moduli are determined from eq 13 by fitting the stress−strain curves to the Mooney−Rivlin model.

The moduli are fitted to the MR model for those experiments where the extension exceeded 60%, except at the lowest mass ratio where extensions above 60% were not obtained. For each mass ratio, at least two (in average three) independent experiments were performed. For each experiment, the equilibrium modulus was fitted to the experimental stress−strain curves.

The MR constants and the moduli with standard deviations can be seen in Table 3. The standard deviations on the experimental determined equilibrium moduli are low, whereas the standard deviations on the C_1 and C_2 constants are fairly large.

The samples prepared at 70 °C were compared to the samples prepared at ambient temperature, and no significant difference was found. This ensures us that the amount of side reactions is kept low despite a relatively high curing temperature.

In Figure 3 a typical stress−strain curve for a sample

Table 3. Equilibrium Moduli and MR Constants Determined by Fitting the Stress−Strain Data to the Mooney−Rivlin Model[a]

mass ratio	15	20	25	30	33	35	40	43.7	50
$G/10^5$ Pa	1.58 ± 0.09	1.66 ± 0.02	1.72 ± 0.06	1.80 ± 0.02	1.77 ± 0.02	1.74 ± 0.10	1.07 ± 0.05	0.73 ± 0.06	0.30 ± 0.01
$C_1/10^5$ Pa	0.57 ± 0.02	0.54 ± 0.06	0.65 ± 0.02	0.60 ± 0.02	0.61 ± 0.08	0.55 ± 0.08	0.39 ± 0.04	0.29 ± 0.03	0.16 ± 0.01
$C_2/10^5$ Pa	0.22 ± 0.07	0.29 ± 0.07	0.21 ± 0.06	0.30 ± 0.01	0.28 ± 0.09	0.32 ± 0.12	0.15 ± 0.06	0.07 ± 0.05	−0.01 ± 0.01

[a]Average values and standard deviations are found by averaging over at least two (on average three) independent experiments for each composition.

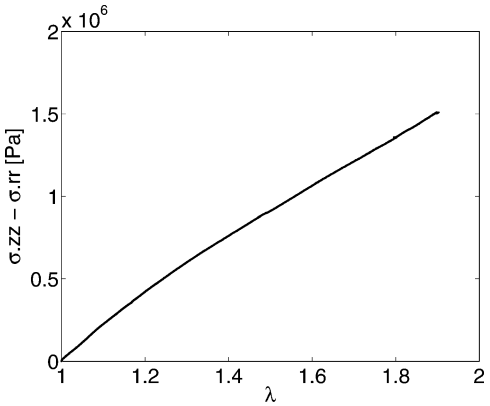

Figure 3. Stress−strain curve for a sample with $m_{DMS}/m_{HMS} = 25$ ($r = 1.73$) at 25 °C.

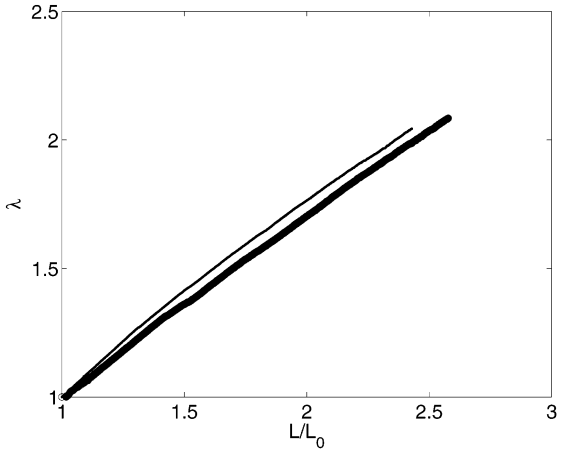

Figure 4. Actual deformation in the middle of the sample (λ) as a function of the applied deformation (L/L_0) for two different samples of the same stoichiometry.

with excess of HMS can be seen. The strain is based on the diameter of the deformed sample, and the stress is the measured force divided by the actual cross-sectional area of the deformed sample at the midpoint. This is in contrast to other data in the literature using engineering stress.[11,28−30] It can be seen in Figure 4 that for two samples from the same reaction mixture (mass ratio 20) that the actual deformation as a function of the applied deformation may vary probably due to slippage. However, the true stress−strain relations of the samples are nearly identical.

It is furthermore observed that for the eight-functional network the response is almost linear. This is expected if $2C_1$ and $2C_1 + 2C_2$ are identified with the shear moduli predicted by the phantom and affine models, respectively.[11] In that case, the ratio $C_1/(C_1 + C_2) = (f - 2)/f$, which for our eight-functional cross-linker takes the value 0.75. It can, however, be shown that the least-squares difference between $3G(\lambda - 1)$ (Hookean linear behavior) and $(C_1 + C_2/\lambda)(\lambda^2 - 1/\lambda)$ over the interval $1 < \lambda < 2$ is minimal for $C_1/(C_1 + C_2) = 0.76$, assuming that $G = 2C_1 + 2C_2$. In fact, the average

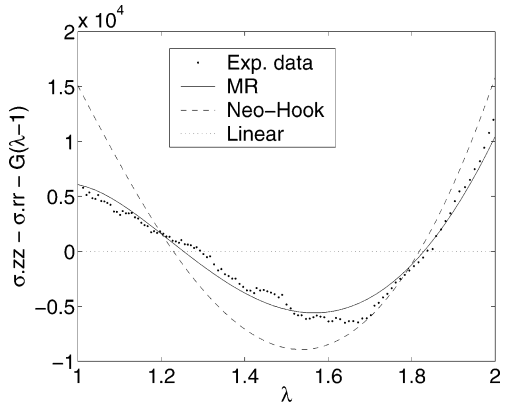

Figure 5. Differences between linear fit and experimental data, Mooney−Rivlin fit, and Neo-Hookean fit. Only every 50th data point is shown. Sample with $m_{DMS}/m_{HMS} = 25$ ($r = 1.73$) at 25 °C.

difference between the linear model and the MR model is only 4% for this value of $C_1/(C_1 + C_2)$. For lower cross-linker functionalities ($f = 4$), the two models deviates already below 25% extension. Hence, precisely for the network we work with, C_1 and C_2 are less accurately determined than the sum of the two: $G = 2C_1 + 2C_2$ is determined from the slope of the stress−strain curve, but the small deviation of this curve from a straight line result in a less accurate determination of C_1 and C_2 individually.

Figure 5 shows a comparison between experimental data and the Hooke, Neo-Hooke, and Mooney−Rivlin models with optimal parameters. On the basis of an F-test, the MR model fitted the data significantly better than the other models in all cases.

One series of Monte Carlo simulations for 38 compositions in the range $0.21 < r < 4.85$ were performed. The Monte Carlo program counts all elastically active chains in the network, but because the cross-linker HMS-301 is entered as a random copolymer, it also contributes elastically active chains. The average distance between cross-link sites on the HMS-301 chain is less than the Kuhn length for DMS. If we for that reason regard HMS-301 as a stiff cross-linker, we need to estimate the number of elastically active DMS-V31 chains alone. For this, we use the calculated values of cycle rank, number of effective edges, and number of vertices as follows: The number of vertices, μ, equals the number of Si-(CH_3)H cross-link sites in the gel particle. The number of edges, ν, equals the number of polymer chains in the gel particle. Ideally, one finds six edges for each four vertices forming a cycle: 1 edge along the HMS-301 chain per vertice and one DMS-V31 edge connecting two vertices. This corresponds to a cycle rank per edge of $^1/_3$ in an ideal network. The cycle rank is defined as $\nu - (\mu - 1)$. Each elastically effective DMS-V31 connects two vertices. For that reason, we find the number of elastically active DMS-V31 edges as $n_{DMS-V31}$ = vertices/2 = (edges − cycle rank)/2, where edges and cycle rank refer

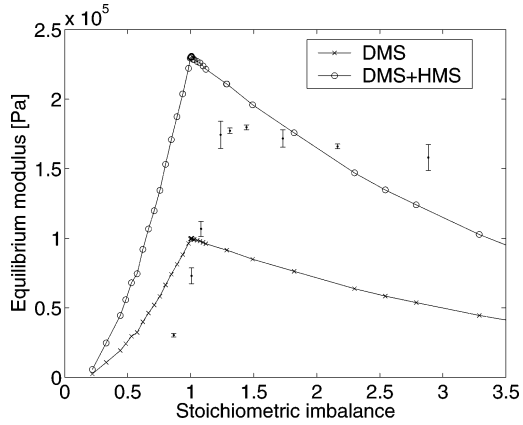

Figure 6. Experimental determined equilibrium moduli as a function of stoichiometric imbalance compared to Monte Carlo simulation results. Average values and one standard deviation are depicted for the experimental data. HMS + DMS is the simulated modulus when both the DMS and the short HMS chains are counted as elastically active. DMS is the modulus when only elastically active DMS chains are taken into account.

only to the elastically active parts of the gel particle. In all simulations, we find the cycle rank per edge to be equal to $^1/_3$, when only elastically active edges are counted. The equilibrium modulus is calculated as $G = [(\text{number of elastically active edges})/V)]kT$. In Figure 6, the results from the Monte Carlo simulations are compared to the experimentally derived equilibrium moduli. From the figure, it is seen that r_{opt} falls within the range $1.25 < r_{opt} < 1.45$. Allowing for a 10% uncertainty in the determination of molecular weights shifts the r values by at least 0.1. Hence, the confidence interval will be $1.1 < r_{opt} < 1.5$. The experimental results are compared to simulation results where only the long DMS chains are taken into account as elastic chains and where both long DMS chains and short HMS chains are counted as elastic chains. Two trends are evident from Figure 6: (1) Up to r_{opt}, Monte Carlo simulations reasonably predict the form of the curve, but the height and position of the curve are wrong. (2) Beyond r_{opt}, the experimental results decrease much slower with r than the simulations. The experimental curve looks as if it is displaced toward higher r values. Even though we do not go near to the gelation limit, both the r values at the gelation point and r_{opt} seem to be displaced by at least 0.25. If the origin of this shift is due to inaccuracy in the structural determination, then either should the molecular weight of DMS be as low as 15 000 g mol^{-1} or more than 30% of the chains should be vinyl terminated in one end only. The maximal modulus predicted by taking only DMS chains into account is less than half the experimental value. The Monte Carlo simulation results depend only on structural imperfections such as dangling ends (and other pendant structures) and loops. It seems most correct to compare simulation results counting elastically active DMS chains only and experimental values. In that case, it is clear that imperfections due to entanglements play a crucial role for the real modulus.

In Figure 7 the experimental determined equilibrium moduli are compared to the prediction of the stochastic model with a locking factor of $L_E = 0.22$, which has been obtained from the model by fitting the value of L_E to the experimental $2C_1$ and $2C_2$ data by means of eqs 15 and 16. A value of $\eta = 0.234$ was assumed. The

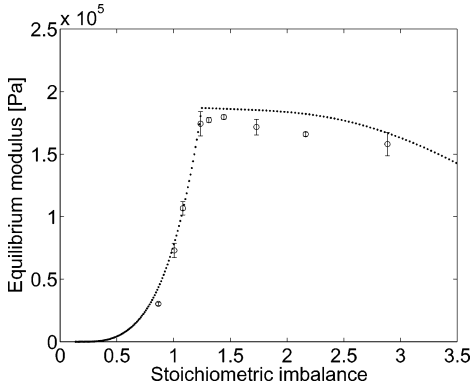

Figure 7. Experimental data for the equilibrium modulus compared to the prediction of the stochastic model assuming one entanglement per DMS chain and a fitted locking factor of $L_E = 0.22$. The stoichiometric imbalance of the stochastic model has been shifted by r_{opt}.

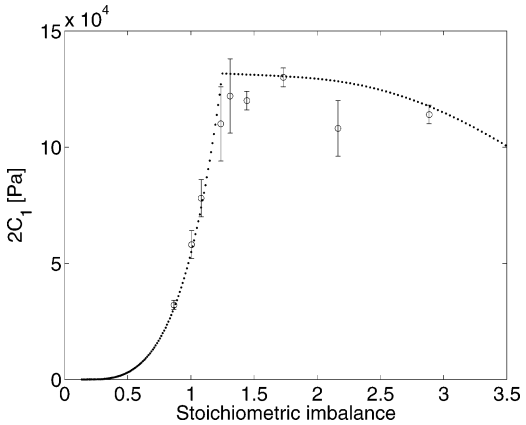

Figure 8. Experimentally determined Mooney−Rivlin constants $2C_1$ compared to the prediction of the stochastic model with a locking factor of $L_E = 0.22$. The stoichiometric imbalance of the stochastic model has been shifted by r_{opt}.

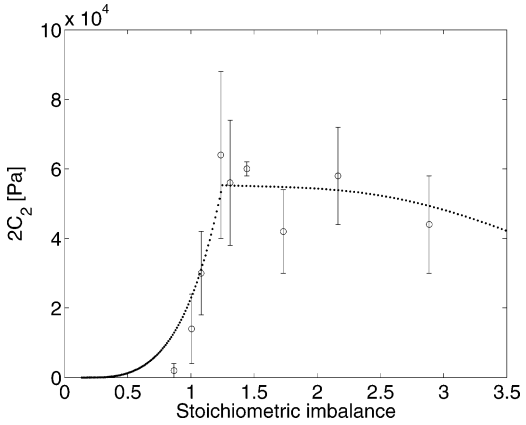

Figure 9. Experimental determined Mooney−Rivlin constants $2C_2$ compared to the prediction of the stochastic model with a locking factor of $L_E = 0.22$. The stoichiometric imbalance of the stochastic model has been shifted by r_{opt}.

stoichiometric imbalance was shifted by a factor of $r_{opt} = 1.3$ in order to compare the results.

In Figures 8 and 9 the experimental values of $2C_1$ and $2C_2$ are compared to the prediction of the stochastic model with the fitted locking factor of $L_E = 0.22$. It is clear that the very simple assumption of one entanglement per DMS chain is capable of explaining the observed trends when the locking factor is fitted. It has to be noted that the choice of the number of entangle-

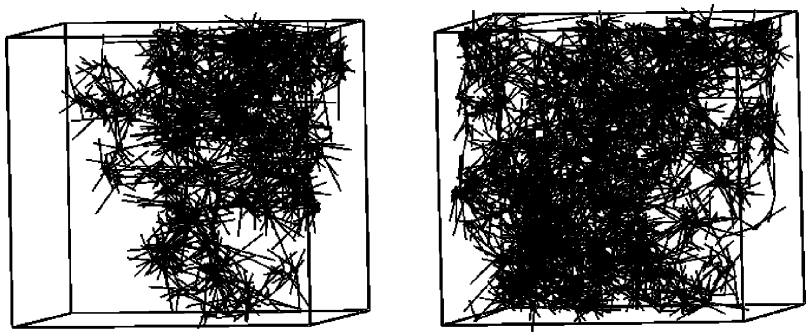

Figure 10. Structure of the largest molecule in the reaction mixture (the gel particle) at the end of reaction calculated for $r = 0.18$ (left) and $r = 0.19$ (right).

Table 4. Gel Point Predictions (r_{gel} = Minimum r Value for Which Gelation Still Occurs)

	Flory−Stockmayer	ARS	stochastic model	Monte Carlo simulations
f_w	8 (13.6)	8 (13.6)	8	
r_{gel}	0.14 (0.08)	0.25 (0.23)	0.14	0.17−0.19

ments per chain shift the curve vertically. It does not change the shape significantly. However, changing the assumption of the number of trapped entanglements being proportional to the square of the number of elastically active DMS chains will change the shape of the curve.

The stochastic model clearly underpredicts the minimum stoichiometric imbalance; a clear evidence of this is seen in Figure 7 as well, but this seems reasonable since the model does not take into account loops. An estimate of the fraction of DMS chains reacting with two HMS sites on the same molecule can be given by calculating the fraction of DMS molecules with their end-to-end radius within the mean-square radius of the HMS molecule:

$$P[r_D < \langle r^2\rangle_H^{1/2}] = \frac{\int_0^{r_H} P(r)\,dr}{\int_0^{nl} P(r)\,dr} = 0.15 \qquad (17)$$

where $[\langle r^2\rangle_i]^{1/2} = (C_\infty n_i l^2)^{1/2}$ with $C_\infty = 6.0$ being the characteristic ratio of DMS, n_i the number of Kuhn segments, and l the Kuhn step length. $P(r)$ is the probability function given by Gaussian chain statistics:

$$P(r) = \left(\frac{3}{2\pi\langle r^2\rangle_D}\right)^{3/2} \exp\left(\frac{-3r^2}{2\langle r^2\rangle_D}\right) \qquad (18)$$

This low value indicates that the single loop formation has a moderate influence on the gel point.

Experimentally, compositions with cross-linker content so low that we approach the gelation limit have not been tested. So the minimum r value for which gelation occurs can only be estimated from Figure 6. The predictions of the gelation limit value from the different simulations and the Flory−Stockmayer[31−34] and Ahmad−Rolfes−Stepto (ARS) theory[35,36] are given in Table 4 to compare the consistency of the different models. In the latter two theories, the weight-averaged functionalities enter the equations. For DMS-V31 this is still two, but for HMS-301 one gets $f_w = 13.6$ if an approximate polydispersity of 1.7 is used. In Table 4, predictions using both $f_w = 8$ and $f_w = 13.6$ are given. The ring-forming parameter in ARS theory is calculated from an end-to-end distance of the smallest ring of 90 Å (corresponding to one DMS-V31 chain). The gel point in the Monte Carlo simulation can be found in several ways: The Accelrys software determines the gel point as the extent of reaction, where more than half of the total mass fraction of reacting chains belongs to the gel particle. Eichinger et al.[7,8] define the extent of reaction from a lower and an upper bound derived from curves of number-average molecular weights vs extent of reaction. Galina and Lechowicz[37] also define the gel point as the extent of reaction, where the sol number-average molecular weight is maximum. Flory−Stockmayer, ARS, and our stochastic model rely on the definition of the gel point as the extent of reaction where a finite probability exists for a given branch point to be connected to infinity. For the Monte Carlo simulation, this definition corresponds to the case where the gel particle is infinite, or alternatively, it fills the whole simulation box. Hence, we define the gel point as the extent of reaction where the gel particle fills the whole simulation box. The minimum r value for which gelation still occurs (r_{gel}) is now defined as the r value where this extent of reaction approaches one. Figure 10 shows the gel particle for r values just below and above r_{gel}. It should be noted that the sol number-average molecular weight shows a maximum as a function of extent of reaction for both of these r values. A simulation where the volume of the simulation box was increased 10 times to 10^{10} Å^3 yielded the same gel point from the visual inspection of the gel particle. The gel particle at $r = 0.18$ was however larger in the big simulation; hence, there may be a tendency toward a slight shift downward in gel point as the simulation size is increased. To compare, Eichinger et al.[17] found that a simulation box with volume 2×10^9 Å^3 yielded satisfactory statistics.

Conclusion

Experimental results show that the strongest network is not obtained for a stoichiometric reaction mixture, but rather for a mixture with an excess of cross-linker. Experimental uncertainties do not suffice to explain this observation.

An almost linear stress−strain relation is obtained for the investigated system. This is a characteristic property for an ideal network composed of eight-functional cross-linkers and end-linked polymer chains. The MC simulations were not capable of describing the shape of the $G(r)$ curve. The stochastic model can explain the trends in MR data when an assumption of one entanglement per DMS chain is made together with the introduction of a fitted locking parameter. This is the fraction of entanglements acting as chemical cross-links, and a value of approximate 0.22 was found. Both simulations predicted $r_{opt} = 1$, although the MC simula-

tions allow for nonideal structures like ring formation, which could explain why r_{opt} should be larger than one. Also surprisingly to us, the MC simulations predicted r_{gel} to be lower than the value predicted by ARS theory. The MC simulations fails to explain the almost constant elastic modulus observed when the excess of cross-linker in the reaction mixture is increased, but this phenomenon can be explained by the number of entanglements being proportional to the square of the number of elastically active DMS chains. An excess of cross-linker ensures that all long end-linked DMS chains are bound in both ends, so the modulus arising from entanglements will stay more or less constant at moderate values of r when $r > 1$.

The effect of entanglements is hardly recognizable for DMS chains with M_n below 30 000 g mol^{-1} due to the fast relaxations in such polymers. The present study shows however that upon cross-linking the presence of entanglements becomes evident as they are trapped during the network formation.

References and Notes

(1) Dutton, S.; Stepto, R. F. T.; Taylor, D. J. R. *Macromol. Symp.* **1997**, *118*, 199−205.
(2) Takahashi, H.; Shibayama, M.; Fujisawa, H.; Nomura, S. *Macromolecules* **1995**, *28*, 8824−8.
(3) Patel, S. K.; Cohen, C. *Macromolecules* **1992**, *25*, 5252−8.
(4) Sivalaisam, K.; Cohen, C. *J. Rheol.* **2000**, *44*, 897−916.
(5) Beshah, K.; Mark, J. E.; Ackerman, J. L. *J. Polym. Sci., Part B* **1986**, *24*, 1207−25.
(6) Gilra, N.; Cohen, C.; Panagiotopoulos, A. Z. *J. Chem. Phys.* **2000**, *112*, 6910−6.
(7) Braun, J. L.; Mark, J. E.; Eichinger, B. E. *Macromolecules* **2002**, *35*, 5273−82.
(8) Stepto, R. F. T.; Eichinger, B. E. In *Elastomeric Polymer Networks*; Mark, J. E., Erman, B., Eds.; Prentice-Hall: Englewood Cliffs, NJ, 1992; pp 256−79.
(9) Rivlin, R. S. *Philos. Trans. R. Soc. London, A* **1948**, *A241*, 379−97.
(10) Edwards, S. F.; Vilgis, T. A. *Polymer* **1986**, *27*, 483−92.
(11) Oppermann, W.; Rehage, G. In *Elastomer and Rubber Elasticity;* Mark, J. E., Lal, J., Eds.; ACS Symposium Series 193; American Chemical Society: Washington, DC, 1982; pp 309−28.
(12) Bach, A.; Rasmussen, H. K.; Hassager, O. *J. Rheol.* **2002**, *47*, 429−41.
(13) Snedecor, G. W.; Cochran, W. G. *Statistical Methods*, 8th ed.; Iowa State University Press: Ames, IA, 1989.
(14) Networks Monte Carlo program in Insight 4.0.0P+, Accelrys, Sept 1999.
(15) Leung, Y. K.; Eichinger, B. E. *J. Chem. Phys.* **1984**, *80*, 3877−84.
(16) Leung, Y. K.; Eichinger, B. E. *J. Chem. Phys.* **1984**, *80*, 3885−91.
(17) Lee, K. J.; Eichinger, B. E. *Macromolecules* **1989**, *22*, 1441−8.
(18) *Polymer Handbook*, 3rd ed.; Brandrup, J., Immergut, E. H., Eds.; John Wiley & Sons: New York, 1989.
(19) Gent, A. N.; Tobias, R. H. *J. Polym. Sci., Part B* **1982**, *20*, 2317−27.
(20) Sharaf, M. A.; Mark, J. E.; Ahmed, E. *Colloid Polym. Sci.* **1994**, *272*, 504−15.
(21) Gottlieb, M.; Macosko, C. W.; Benjamin, G. S.; Meyer, K. O.; Merrill, E. W. *Macromolecules* **1981**, *14*, 1039−46.
(22) Macosko, C. W.; Benjamin, G. S. *Pure Appl. Chem.* **1981**, *53*, 1505−18.
(23) Villar, M. E.; Bibbó, M. A.; Vallés, E. M. *Macromolecules* **1996**, *29*, 4072−80.
(24) Fetters, L. J.; Lohse, D. J.; Milner, S. T.; Graessley, W. W. *Macromolecules* **1999**, *32*, 6847−51.
(25) Thirion, P.; Weil, T. *Polymer* **1984**, *25*, 609−14.
(26) Ball, R. C.; Doi, M.; Edwards, S. F.; Warner, M. *Polymer* **1981**, *22*, 1010−8.
(27) Brereton, M. G.; Klein, P. G. *Polymer* **1988**, *29*, 970−4.
(28) Erman, B.; Flory, P. J. *J. Polym. Sci., Part B* **1978**, *16*, 1115−21.
(29) Termonia, Y. *Macromolecules* **1989**, *22*, 3633−8.
(30) Zhang, L.-X.; Jiang, Z.-T.; Zhao, D.-L. *J. Polym. Sci., Part B* **2002**, *40*, 105−14.
(31) Stockmayer, W. H. *J. Chem. Phys.* **1943**, *11*, 45.
(32) Stockmayer, W. H. *J. Chem. Phys.* **1944**, *12*, 125.
(33) Flory, P. J. *J. Am. Chem. Soc.* **1941**, *63*, 3083.
(34) Flory, P. J. *Principles of Polymer Chemistry*; Cornell University Press: Ithaca, NY, 1953; pp 347−398.
(35) Ahmad, Z.; Stepto, R. F. T. *Colloid Polym. Sci.* **1980**, *258*, 663−74.
(36) Rolfes, H.; Stepto, R. F. T. *Makromol. Chem., Macromol. Symp.* **1993**, *76*, 1−12.
(37) Galina, H.; Lechowicz, J. B. *Macromol. Symp.* **2001**, *171*, 37−44.

MA034355P